Appl. Phys. B (2014) 116:313–323
DOI 10.1007/s00340-013-5692-y

Applied Physics B
Lasers and Optics

Experimental study of the $E(m, \lambda)/E(m, 1064)$ ratio as a function of wavelength, fuel type, height above the burner and temperature

S. Bejaoui · R. Lemaire · P. Desgroux · E. Therssen

Received: 16 May 2013 / Accepted: 11 October 2013 / Published online: 30 October 2013

Abstract The optical properties of soot have been studied for many years with a particular attention focused on refractive index. In the present study, the two-excitation wavelength laser-induced incandescence technique has been applied to determine the ratio of the soot absorption function as a function of the wavelength. The advantage of this technique is to provide the determination of the $E(m)$ ratio using a non-intrusive laser-based method without being disturbed by scattering. Measurements have been carried out in a methane premixed flat flame and in a diesel turbulent spray one. Four pairs of wavelength have been used to evaluate the spectral behavior of $E(m)$ ratios from ultraviolet (UV) to near infrared (NIR). The two-excitation wavelength LII method implies heating soot the same way using two different laser excitations. Particular operating conditions must be selected to insure the equality of the LII signals, such an equality being necessary to derive the $E(m)$ ratio. A laser excitation at 1064 nm has been chosen as a reference, and the obtained results have been compared with those issued from the use of UV and visible wavelengths of 266, 355, 532 and 660 nm. Results show a significant decrease of the $E(m)$ ratio from UV to visible while it tends to become constant from 532 nm to NIR. The use of different experimental conditions allows to analyze the dependence of the $E(m)$ ratios with the height above the burner, the fuel type and the soot temperature. No significant influence of these parameters has been pointed out on the relative $E(m)$ values determined in the flame conditions investigated here.

List of symbols

d_p (m)	Soot primary particles diameter
$E(m, \lambda)$	Soot absorption function
F_λ (J m^{-2})	Laser fluence
E_λ (J)	Total energy of the laser pulse radiation
f_v	Soot volume fraction
H_{abs} (W)	Absorbed power of a single soot particle
$m = n - ik$	Optical index
Q_{abs}	Soot absorption efficiency
q_λ (W m^{-2})	Laser irradiance
S_{laser} (m^2)	Laser pulse cross-sectional area
T (K)	Particle temperature
λ (m)	Wavelength
δt (s)	Laser pulse duration

Abbreviations

Diester	Diesel/rapeseed methyl ester (RME) mixture
HAB	Height above the burner
LIF	Laser-induced fluorescence
LII	Laser-induced incandescence
PAH	Polycyclic aromatic hydrocarbon
TEM	Transmission electron microscopy
TiRe-LII	Time-resolved LII

S. Bejaoui (✉) · R. Lemaire · P. Desgroux · E. Therssen
Université Lille Nord de France, 59000 Lille, France
e-mail: salmabejaoui@hotmail.fr

S. Bejaoui · P. Desgroux · E. Therssen
CNRS UMR 8522, PC2A, Université Lille 1,
59655 Villeneuve d'Ascq, France

R. Lemaire
EMDouai, EI, 59500 Douai, France

1 Introduction

Soot particles produced in fuel-rich combustion conditions can affect the radiation budget of the atmosphere. This is mainly due to absorption and scattering processes of solar radiations and infrared thermal radiation of the earth's surface [1]. Many laboratories working in the fields of atmospheric chemistry and ecology have thus focused their researches on the study of optical properties of soot particles. A major part of the works conducted on that topic have been carried out in laboratory flames to directly quantify the refractive index of soot (m) or to indirectly evaluate the soot absorption function ($E(m)$). Experimental determination of the optical properties of soot has been evaluated by both in situ [2–5] and ex-situ [6–8] measurements. This partly explains the wide discrepancy in the values of m or $E(m)$ reported in the literature.

Reviews regarding empirical and semiempirical investigations dealing with soot optical constants are available in [9, 10]. Large uncertainties in the spectral dependences of these properties emerged from the reported trends and results. Several studies proposed that the refractive index of soot and then the absorption function are wavelength-independent. Snelling et al. [11] especially suggested that the $E(m)$ function was constant in the 500–945 nm wavelength range. Assuming that the $E(m)$ function is wavelength independent is commonly used in the literature for pyrometric temperature measurements in flames [12–14]. The choice of the two or three wavelengths selected for such measurements is still subject to great debates particularly when the wavelength window used for the detection is below 500 nm [15]. To avoid biases induced by this approximation, wavelength-dependent absorption functions have been proposed in the literature. The most used spread relation is the one issued from the work of Chang and Charalampopoulos [16]. It is derived from measurements carried out in a propane-oxygen flame. These authors proposed a spectral evolution of m in the 400–3000 nm wavelength range. The obtained evolution of the $E(m)$ function shows a decreasing behavior up to the NIR followed by an increase for longer wavelengths. Other semi-empirical models have been proposed in different works [6, 17, 18]. They predict a different spectral evolution of the $E(m)$ compared to that depicted by Chang and Charalampopoulos. According to models proposed by Dalzell and Sarofim [6] and Lee and Tien [17], $E(m)$ decreases significantly from UV to 500 nm while it increases slightly in the range of wavelength up to 700 nm.

Besides uncertainties derived from each technique implemented to estimate the spectral behavior of $E(m)$, both sensitivity of soot optical parameters to flame conditions [7, 16, 19] and particles morphology [7, 20] are key parameters that may explain discrepancies in the models proposed in the literature. Recently, several studies attempted to highlight the evolution of optical parameters of soot particles according to their growth process. The first one, conducted by Henriksen et al. [7], provides an evolution of the real and imaginary part of the soot refractive index as a function of the HAB in a benzene inverse diffusion flame. Based on ex-situ reflectance measurements and FTIR analyses, Henriksen et al. found that the optical properties of soot increase as a function of the height in the flame (i.e., as a function of the soot maturation stage). Bladh et al. [20] also reported a similar evolution of the $E(m, \lambda)$ function with the HAB by combining LII signals modeling and TEM analyses in a premixed atmospheric flame of ethylene.

At this point, it should be noted that soot optical constants are usually calculated assuming soot as individual spherical particles. If aggregation is not active, interaction of light with particles is described in the Rayleigh regime where absorption is predominant in comparison with scattering phenomenon. On the other hand, the use of the Rayleigh-Debye-Gans model for fractal aggregates (RDG-FA) emerges as being a good compromise between accuracy and simplicity when particles are agglomerated. Radiative properties of fractal soot aggregates have received considerable attention during the past decades [21–23]. For instance, Farias et al. [21] compared extinction coefficients calculated for aggregates and primary particles. They observed an unexpected behavior in the UV and infrared wavelength regions. Such an evolution may be correlated with the effect of the aggregation process on the spectral evolution of optical parameters. It may then enhance uncertainties associated with the determination of these parameters.

There are still outstanding issues regarding the evolution of the soot optical properties as a function of the wavelength, the soot maturity stage or the fuel used. The aim of the present experimental work is thus to study the wavelength dependence of soot absorption from UV to NIR. We used the two-excitation wavelength laser-induced incandescence technique that has been developed in our team [24]. This technique is a non-intrusive laser-based method which allows the determination of the relative value of $E(m)$ without being disturbed by scattering. Previous investigations were carried out in different flame conditions with two wavelength pairs providing ratios of the absorption function at 532/1064 nm [8, 25–27] and 266/1064 nm [8, 28]. In the present paper, we applied this method in two atmospheric flames: a premixed gaseous one and a turbulent diesel spray flame. New wavelength pairs have been used to evaluate the relative spectral behavior of $E(m)$. Excitation at 1064 nm has been chosen as a reference, and results have been compared with those obtained with UV and visible wavelengths of 266, 355, 532 and

660 nm. Finally, probing two types of flame at different heights and with different laser fluences allowed to discuss and analyze the dependence of the $E(m)$ ratios with the HAB, the fuel type and the soot temperature.

2 Methodology

The two-excitation wavelength laser-induced incandescence technique is described in detail in [8, 24]. Consequently, this section only briefly presents its main principle. It focuses more on discussions regarding the cautions and conditions required to apply it.

The two-excitation wavelength LII technique consists in heating soot particles the same way by selecting laser energies for two different excitation wavelengths ensuring that soot particles absorb the same amount of energy. Hence, particles reach the same temperature and emit the same LII radiation. In this work, emissions collected with a laser excitation at 1064 nm have been taken as a reference and compared with those obtained using UV or visible excitation wavelengths. Consequently, it will always be referred to this particular wavelength in the following equations.

For a given spatial position, the equality between the energy absorbed with the two-excitation wavelength can be written as:

$$\int_{\delta t} H_{\text{abs}}(t, \lambda) \cdot \mathrm{d}t = \int_{\delta t} H_{\text{abs}}(t, 1064\ \text{nm}) \cdot \mathrm{d}t \tag{1}$$

where the power absorbed by the particle (H_{abs}) during the pulse duration (δt) is given by:

$$H_{\text{abs}}(t, \lambda) = Q_{\text{abs}}(t, \lambda) \cdot \frac{\pi \cdot \mathrm{d}_p(t)^2}{4} \cdot q_\lambda(t) \tag{2}$$

q_λ being the laser irradiance and Q_{abs} the absorption efficiency. In the Rayleigh limit assumptions, the absorption efficiency can be written as:

$$Q_{\text{abs}}(t, \lambda) = E(m, \lambda) \cdot \frac{\pi \cdot \mathrm{d}_p(t)}{4} \tag{3}$$

Sublimation is not active at low laser fluence. The particle diameter is thus assumed to be identical for each wavelength at each time of the LII process. By combining Eqs. 2 and 3, the equality of the absorbed energies then becomes:

$$\frac{E(m, \lambda)}{\lambda(\text{nm})} \cdot \int_{\delta t} q_\lambda(t) \cdot \mathrm{d}t = \frac{E(m, 1064\ \text{nm})}{1064} \cdot \int_{\delta t} q_{1064\ \text{nm}}(t) \cdot \mathrm{d}t \tag{4}$$

The integral of the irradiance ($q_\lambda(t)$) over the entire laser pulse is equal to the total energy (E_λ) divided by the section of the beam (S_λ).

$$\int_{\delta t} q_\lambda(t) \cdot \mathrm{d}t = \frac{E_\lambda}{S_\lambda} \tag{5}$$

Then, Eq. 4 becomes:

$$\frac{E(m, \lambda)}{\lambda(\text{nm})} \times \frac{E_\lambda}{S_\lambda} = \frac{E(m, 1064\ \text{nm})}{1064} \times \frac{E_{1064\ \text{nm}}}{S_{1064\ \text{nm}}} \tag{6}$$

Using the same spatial distribution of the laser irradiance for both excitations, the ratio of $E(m)$ can be written as a function of the ratios of the selected wavelengths and laser energies.

$$\frac{E(m, \lambda)}{E(m, 1064\ \text{nm})} = \frac{\lambda(\text{nm})}{1064} \cdot \frac{E_{1064\ \text{nm}}}{E_\lambda} \tag{7}$$

To apply this technique, the operating conditions must be selected carefully in order to fulfill the following conditions:

1. Spatial distributions of the laser pulse energy must be identical for the two-excitation wavelength. Furthermore, both pulses must be perfectly coincident to excite identical volumes of soot particles (Eq. 5).
2. Temporal profiles of the laser pulses must be identical for the two selected wavelengths in order to excite soot with identical pulse durations (Eq. 1). For instance, Fig. 1 shows the evolution of the peak LII signal as a function of the laser fluence (so-called fluence curves) using two laser pulses at 1064 nm. Laser beams have very different temporal profiles with full width at half maximum (FWHM) of 7 and 11 ns. As one can see, when the FWHM of the pulse is lower and thus its peak power is higher, soot reached higher temperature and this greatly influences the obtained results.
3. The delay between the beginning of laser pulses and the beginning of the acquisition of signals must be the same mainly when the two excitations are emitted by different sources. Such a parameter is indeed of importance to be able to compare signals at the same time of the LII process.

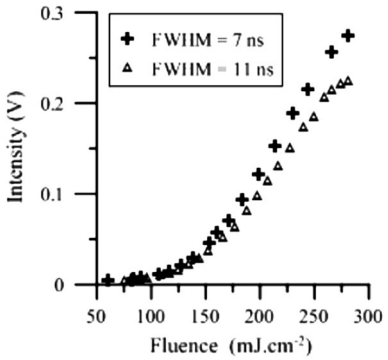

Fig. 1 Fluence curves obtained with 1064 nm pulses having FWHM of 7 and 11 ns

4. The collection systems must have the same spectral efficiencies.
5. Measurements must be carried out in the low fluence regime to avoid the activation of the sublimation process. Furthermore, using low fluence permits avoidance of other non-thermal phenomenon such as C_2 clusters photodesorption [29] that involves processes that are different depending on the wavelength used. Thus, selecting such operating conditions (i.e., fluences below the sublimation threshold) allows focusing the analysis on the thermal history of soot only.

3 Experimental setup

3.1 Burners and flames

Two types of flame have been investigated in this work.

First, measurements have been carried out in a premixed gaseous flame stabilized on a McKenna burner at atmospheric pressure. The total flow rates of methane, oxygen and nitrogen are 2.47, 2.3 and 5.17 Nl/min, respectively. The equivalence ratio Φ was thus of 2.15. It was shielded with a co-annular air flow to avoid perturbations from ambient atmosphere. A flame stabilizer made of stainless steel was placed at a distance of 20 mm above the burner.

The second flame has been stabilized on a McKenna hybrid burner described in [30]. The porous plug of this burner contains a central hole allowing the introduction of a coaxial atomizer (DIHEN). A mass flow rate of 46 g/h of diesel was introduced into this atomizer and pulverized with a nitrogen flow of 0.32 l/min. This generates a spray of micron-sized fuel droplets characterized in [30]. A premixed methane/air flat flame (equivalence ratio $\Phi = 0.8$) stabilized on the porous plug then allows the vaporization and ignition of the liquid fuel droplets. It generates a turbulent diffusion flame of 18 cm height and 2 cm width with no trace of liquid fuel above 12 mm HAB.

3.2 Laser and beam shaping

Different experimental setups (represented in Fig. 2) have been used to measure the ratios of the soot absorption functions with four wavelength pairs. As mentioned above, a laser source at 1064 nm generated by a Quantel Brilliant B laser has been used as a reference excitation. The second laser source has been chosen in the UV (266 and 355 nm) or in the visible (532 and 660 nm). The fourth harmonic (266 nm) and the second harmonic (532 nm) of the 1064 nm laser excitation source have been generated using the Nd:YAG (Quantel Brilliant B). Laser pulses at 355 nm have been generated using the frequency tripler of a continuum laser (Powerlite 8000 Continuum) while laser excitation at 660 nm was emitted by an OPO (Panther Ex OPO continuum) pumped by the third harmonic of the Continuum YAG. The two last wavelengths (355 and 660 nm) have a much larger pulse duration than those generated by the Quantel laser. Thus, when using the 355/1064 nm or the 660/1064 nm configurations, the temporal profile of the laser source at 1064 nm (Quantel Brilliant B) was broadened by changing the delay between the flash lamps and the Q-Switch. By this way, it has been possible to obtain an identical pulse duration for both excitations (FWHM = 11 ns) in each configuration.

For each pair of laser wavelengths, laser beams were perfectly aligned in parallel with the burner and identically shaped. We used a tophat spatial profile for 355/1064 nm and 660/1064 nm configurations. The central portion of each beam sections was then selected with a rectangular slit and relay imaged to the center of the burner using a 200-mm focal lens.

The homogeneity of the laser sources at 266 and 532 nm did not allow the generation of tophats with a uniform fluence. Hence, we used an Airy diffraction profile for 266/1064 nm and 355/1064 nm configurations. Such profiles were generated by filtering lasers with a 1-mm diaphragm. By adjusting distance between the diaphragm and the center of the burner for both excitation wavelengths, an identical spatial profile was obtained [24] (Fig. 2).

For each configuration, the spatial distribution for both wavelengths was thoroughly monitored before measurements using a CCD beam profiler (Gentec beamage).

3.3 LII setup

Temporally and spectrally resolved measurements were acquired to measure the ratios of the soot absorption function for each configuration. Laser-induced emissions were focused using a set of two achromatic lenses ($f1$ = 200 mm and $f2$ = 600 mm) at the entrance of a spectrograph (Acton 300 i) with a 150 g/mm 300 nm blazed grating. This spectrograph is equipped with two exit ports. The first one is used for the detection of signals with the ICCD camera and the second one for temporally resolved measurements with the photomultiplier tube (PMT).

At the entrance of the spectrograph, a rectangular slit of 1.5 mm height (y) and 7 mm width (z) has been used and aligned in parallel with the horizontal surface of the burner. Considering the resulting optical magnification (3:1), the collection volume is 2.33 mm long in the direction of the

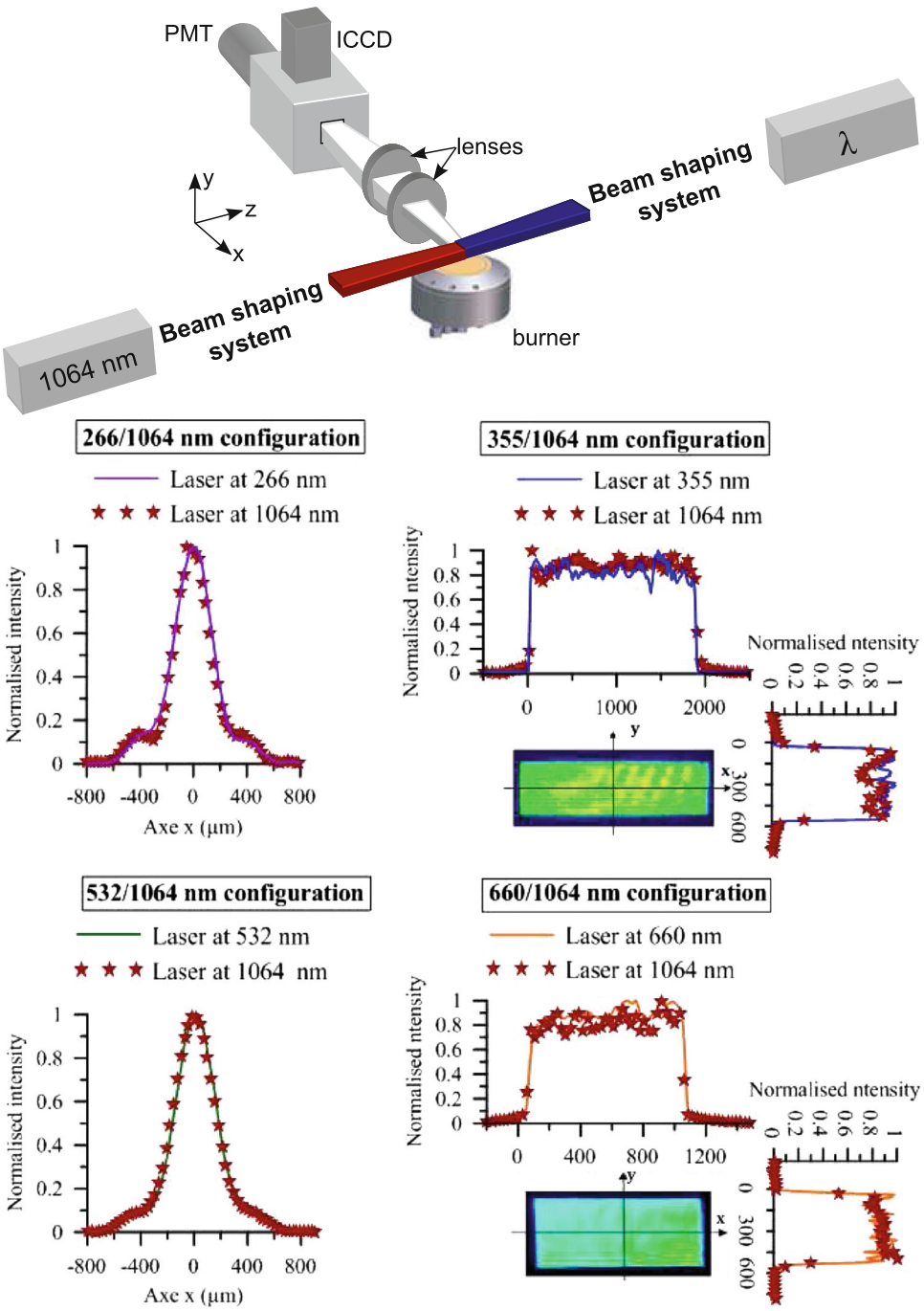

Fig. 2 Experimental setup and spatial profiles of shaped beams for each configuration

laser beam and covers the entire section of the laser sources. Spectra were recorded using an ICCD camera (Princeton PiMAX) placed at the exit of the spectrograph by binning all sensor elements of the chip perpendicular to the wavelength axis. The gate width of the camera is set to 50 ns for all measurements. The spectrograph has been calibrated using spectral lines from a mercury emission lamp (Oriel 6035). The spectral response of the detection setup has been corrected using an optical sphere (SphereOptics CSTM-LR-6-M) that emits a blackbody radiation and allows working with different sets of temperature up to 3220 K. The optical setup and solid angle are the same for the calibration procedure and for the detection of soot emissions.

TiRe-LII measurements were performed with a PMT (Philips XP 2237 B) placed after the second exit slit of the spectrograph. Depending on grating position and exit slit width, adjustable spectral width of detection could

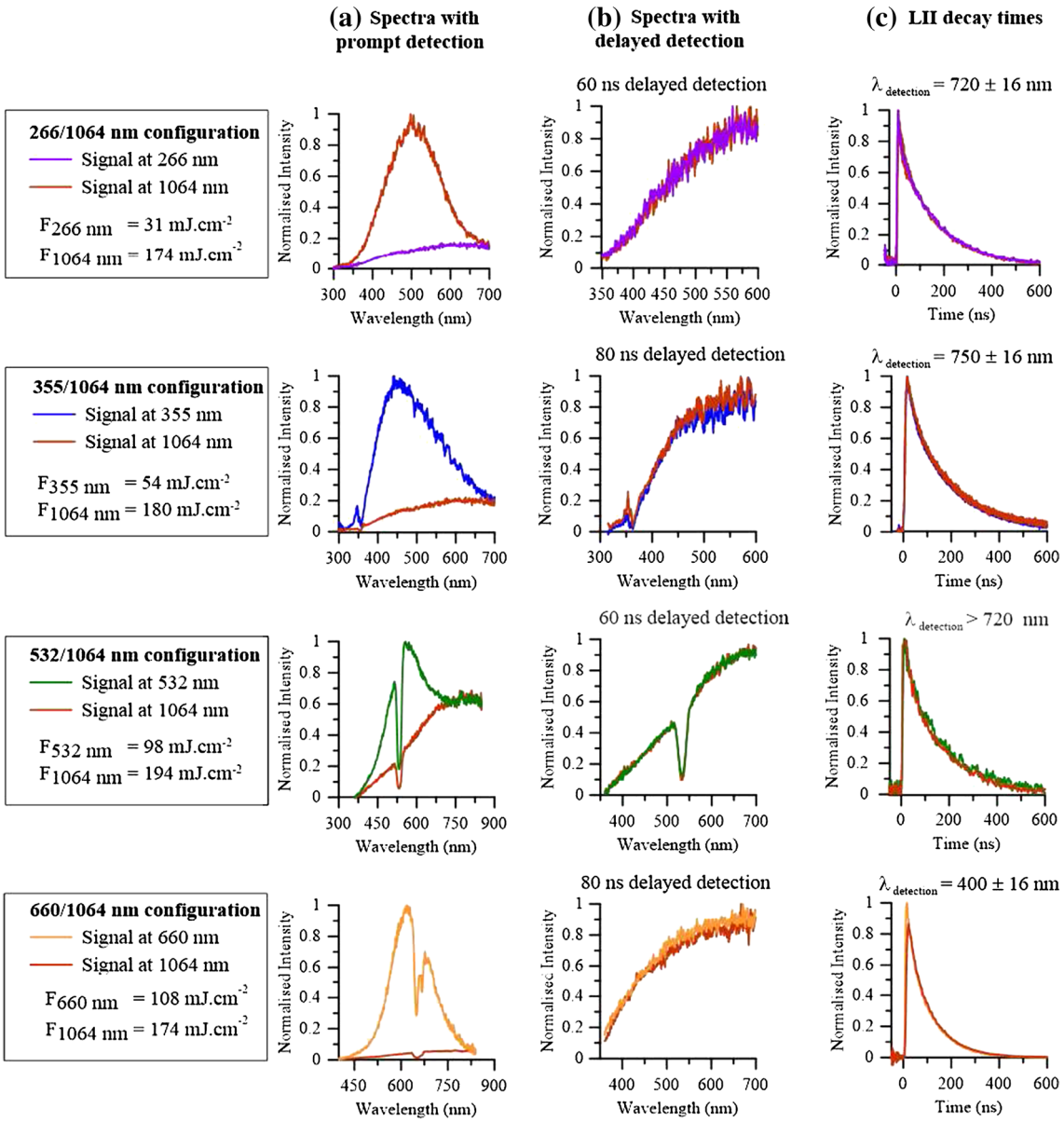

Fig. 3 Application of the two-excitation wavelength technique using 266/1064 nm, 355/1064 nm, 532/1064 nm and 660/1064 nm configurations. Measurements are performed at 15 mm HAB in the premixed flat flame. **a** Spectra of the laser-induced emission for both laser excitations with a prompt detection. **b** LII spectra delayed by 60 ns (for 266/1064 nm and 532/1064 nm configurations) or 80 ns (for 355/1064 nm and 660/1064 nm). **c** LII time decays for both laser excitations with a selected band of detection for each configuration

be obtained. Five hundred LII time decays were averaged on a digital oscilloscope (Lecroy technology, 500 MHz bandwidth, 2.5 GS/s sampling rate) triggered by the signal provided by a photodiode (Thorlabs DET 210). The spectral response of the photodiode is comprised between 200 and 1000 nm, and its rise time is of 2 ns.

Finally, the extinction of the laser through the flame has been found to be negligible whatever the wavelength used. Consequently, the laser energy has been measured using a power meter located behind the flames.

4 Results and discussion

4.1 Interference between laser-induced fluorescence and incandescence

PAHs are present in the sooting zone of the premixed flat flame. Thus, laser-induced emissions, following UV or visible laser excitations, can be assigned to either LIF of PAH (or more generally LIF of soot precursors) or to LII.

Figure 3a shows laser-induced emission spectra measured at 15 mm HAB for each configuration, the gate width

of the ICCD camera being timed to start when the first photons of the laser are emitted (prompt detection). Soot precursors are transparent to 1064 nm excitation. Thus, the signal detected with this laser is assigned to LII signals emitted by soot. However, signals induced by the second wavelength excitation shows an additional broadband emission attributed to the fluorescence of soot precursors. This fluorescence emissions collected for each studied configuration directly depends on the wavelength of the laser excitation. LIF signals extend from 300 to 650 nm using 266 and 355 nm excitations. With laser at 532 nm, soot precursors emit a LIF signal from 370 to 720 nm. Finally, even with a 660 nm excitation, a broadband emission that we also attribute to soot precursors LIF can be observed from 450 to 780 nm. Works are in progress in our laboratory to discuss and analyze this unexpected fluorescence emission.

One can note sharp wavelength cut-offs on the spectra obtained for the three last configurations. This is due to the use of negative filters placed in front of the spectrograph to reject laser scattering at 355, 532 and 660 nm.

4.2 Spectral dependence of the ratio of $E(m)$

Two experimental procedures have been implemented in order to avoid the interference of LII emission with LIF signals of relatively short duration (less than 80 ns). In the case of spectral measurements, the detection of the signals has been delayed from the start of the laser pulse by 60 or 80 ns for both excitations (Fig. 3b) depending on the temporal profiles of the laser pulses.

For time-resolved measurements, the spectral band used for the detection has been chosen for each wavelength pair in order to remove radiations emitted by soot precursors. For the 266/1064 nm and 355/1064 nm configurations, the detection spectral bands have been selected by centering the grating at 720 and 750 nm, respectively. With the 532/1064 nm configuration, the spectrograph was removed and LIF emissions were filtered with a long-pass filter to collect signals above 720 nm only. Finally, for the 660/1064 nm configuration, a detection centered at 400 nm allows a significant reduction in the interferences between LIF emission and collected LII signals.

For each configuration, the energy at 1064 nm has been fixed so that the laser fluence is below the sublimation threshold (i.e., in the low fluence regime). We then adjusted the fluence of the second excitation source to obtain identical temporal and spectral LII signals. Since the required experimental conditions summarized in Sect. 3.2 are fulfilled, the coincidence of the LII time decays and spectra shown on Fig. 3 indicates that the selected laser fluences allow heating soot particles the same way. Furthermore, the fact that time decays are identical for each pair of wavelengths demonstrates that the soot thermal history is identical in each case. Ratios of $E(m)$ can then be deduced using Eq. 7. The obtained results are plotted in Fig. 4 and compared with data issued from several works based on ex-situ [6, 8] and in situ measurements [5, 8, 11].

First, we can note that the $E(m, 532\text{ nm})/E(m, 1064\text{ nm})$ ratio issued from the present study is in good agreement with values previously obtained using the same method in different atmospheric flames [8, 24, 26, 28] or in a recent experimental work from Michelsen et al. [32, 33].

The present study shows that the $E(m)$ ratio is constant above 532 nm which is in good agreement with observations from Snelling et al. [11]. Nevertheless, this trend is inconsistent with that depicted by other models as shown in Fig. 4. Yon et al. [8] proposed that the relative evolution of the $E(m)$ was wavelength independent above 800 nm. The model proposed by Chang and Charalampopoulos [16] suggests that $E(m)$ gradually increases from visible up to NIR.

On the other hand, our results show a significant decrease of the $E(m)$ ratio from UV to visible. According to this observation, the absorption efficiency of soot appears to be more important in the UV region which might be correlated with the fact that soot particles still contain chemical functionalities behaving like aromatic structure [34].This trend is moreover consistent with models from Dalzell et al. [6], Yon et al. [8] and other results not reported in Fig. 4 [17, 18].

4.3 Dependence of the $E(m)$ ratio with the soot maturity

Aging of soot has been observed during numerous transmission electron microscopy (TEM) analyzes showing that nascent particles exhibit poor contrast compared to mature soot [20, 35, 36]. De Iuliis et al. [35] noted during TEM grids observation that nucleated soot present a spherical-cup geometry, a liquid-like structure and a tendency to spread over the substrate surface. Based on these observations, it seems realistic to assume that optical properties of soot probably change with these structure evolutions. Different investigations have thus been performed during the last decade to discuss more in detail such variations. Bladh et al. [20] studied the variation of the soot absorption function as a function of the HAB in a premixed one-dimensional ethylene/air flame stabilized on an atmospheric McKenna burner. On the basis of LII time decays modeling, TEM analysis and rotational CARS thermometry, the authors of this work found an increase of 53 % of the absolute $E(m)$ value with increasing HAB. Using a two-color excitation laser-induced incandescence method, Cléon et al. [27] determined the evolution of the $E(m, 532\text{ nm})/E(m, 1064\text{ nm})$ ratio as a function of the height in

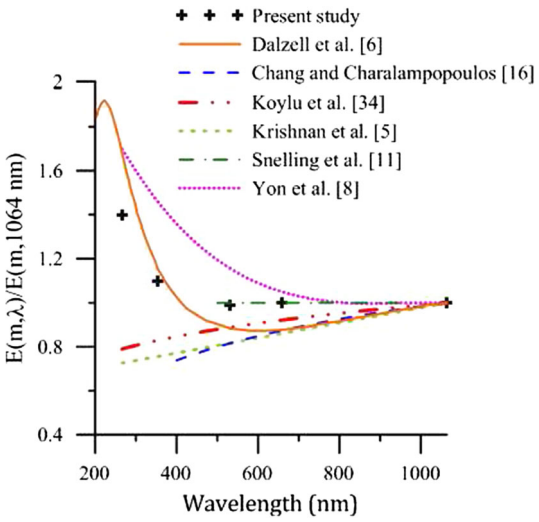

Fig. 4 Wavelength dependence of the ratio of soot absorption function. Results from present work are compared with data issued from [5, 6, 8, 11, 16, 31]

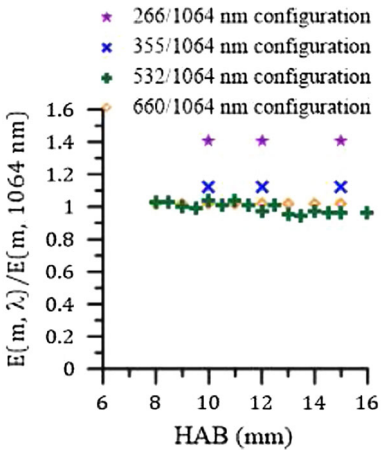

Fig. 5 Dependence of the $E(m)$ ratio with HAB

a low-pressure premixed methane flame. Authors observed a monotonic decrease of this ratio in the early sooting region. A constant value was then obtained at higher heights. This finding suggests a variation of the optical properties of soot during their maturation process, the stabilization of the $E(m,\ 532\ \text{nm})/(E(m,\ 1064\ \text{nm})$ ratio observed at high HAB being correlated with the apparition of mature soot.

In the present work, we studied the evolution of the $E(m)$ ratio as a function of the HAB in the premixed atmospheric flame using four wavelength pairs. Ratio of $E(m)$ displayed in Fig. 5 is deduced by overlaying LII spectra with delayed detection for both excitations at different HAB. $E(m)$ ratios were also obtained with TiRe-LII measurements by overlaying LII time decays with both excitations.

The obtained results show that the $E(m)$ ratio is constant for all the investigated heights in the premixed flame even with the 266/1064 and 355/1064 nm configurations. Such a trend is noteworthy since one could have supposed that the maturation stage of soot would have influenced their absorption behavior in UV (the absorption function in the UV being wavelength dependent as demonstrated in Fig. 4). On the other hand, it should be noted that the absolute value of the $E(m)$ function probably changes with the maturation stage of soot. Thus, our results only indicate that the $E(m)$ ratio is constant with the HAB. Compared to the results obtained by Cléon et al. [27], we do not observe regions of the flame where the $E(m)$ ratio varies and tends to a constant value. This is probably due to the fact that the soot nucleation region is spatially expanded to few millimeters in low-pressure flame conditions which is not the case in atmospheric flame where this region is too thin to be thoroughly probed.

Finally, it should be noted that the two-excitation wavelength laser-induced incandescence technique is based on the Rayleigh limit assumption as mentioned in Eq. 2. It is well known that soot formation in a premixed flat flame can be followed in time from the initial particle inception, via surface growth and coagulation, to aggregation and agglomeration. Finding that $E(m)$ ratios are constant regardless of the height in the flame suggests that the aggregation does not affect the spectral dependence of the ratio of $E(m)$ in our flame conditions, a behavior that was already observed in previous works related to the study of turbulent liquid fuels spray flames [8, 25, 26, 28].

4.4 Dependence of the $E(m)$ ratio with the fuel type

Results regarding the effect of the fuel type on the soot refractive index show some discrepancies and uncertainties. Early works of Dalzell and Sarofim [6], Lee and Tien [17] and Köylü et Faeth [31] suggest that the optical properties of soot do not change significantly from flame to flame despite the different H/C ratios of the fuels used in these studies. On the other hand, investigations reported by Habib and Vervisch [18] or Charalampopoulos et al. [3] indicate that the influence of the fuel type on the soot refractive index is not negligible. To investigate this point, we also applied the two-excitation wavelength laser-induced incandescence technique in a turbulent diffusion flame of diesel at different heights above the burner. We present in Fig. 6 the spectra obtained with a prompt detection for the 355/1064 nm and 532/1064 nm configurations. Three typical HAB have been probed. At 20 mm HAB, soot particles are not formed yet and the spectra collected at 355 or 532 nm are only assignable to LIF emissions from soot precursors. At 110 mm above the burner, the obtained spectra are identical for both

excitations for all the wavelength pairs used. This indicates that there is no fluorescence emission any more. This also indicates that soot particles reached the same temperature with the two laser excitations. Soot particles and soot precursors coexist for an intermediate HAB of 70 mm. Therefore, one can observe the superposition of a LIF contribution to the LII spectra for wavelengths comprised between 350 and 700 nm. Nevertheless, the signals collected at 70 mm perfectly fit for longer wavelengths (above 700 nm) when using laser fluences identical to those chosen to obtain the spectra collected at 110 mm HAB. This confirms the validity of the selected laser fluence pairs and this shows once more that the $E(m)$ ratio is constant regardless of the height in the flame.

The $E(m)$ ratios obtained in the diesel flame are consistent with those measured before in the premixed flame. Furthermore, the value of the $E(m,\ 532\ \text{nm})/E(m,\ 1064\ \text{nm})$ ratio obtained here is consistent with that derived from measurements carried out in a premixed acetylene/air flame [24] and in various liquid fuels flames [8, 25, 26, 28]. By the same way, the $E(m, 266\ \text{nm})/E(m, 1064\ \text{nm})$ values obtained here in both types of flame is perfectly coincident with data issued from the analyses of diesel and Diester flames [8, 28]. Since similar results are obtained in all these different flames, we can estimate that the $E(m)$ ratio of in-flame soot seems to be relatively insensitive to the fuel type.

4.5 Dependence of the $E(m)$ ratio with the temperature

The soot absorption function ratios can also be derived using an energetic approach [8, 24, 27] consisting in comparing the fluence curves obtained for each laser excitation wavelength with the same detection conditions (detection delayed by 60 or 80 ns in the present case). Figure 7a displays the fluence curves recorded for three wavelength pairs at 15 mm HAB in the premixed methane flame. The fluence at 1064 nm has always been chosen as a reference and we applied translation factors to the abscissa scale of the second fluence curves presented on Fig. 7b to obtain an overlap of the two curves at low fluence regime. Such a shifting procedure is explained in detail in [8]. According to Eq. 7, the translation factor (5.5 for the 266/1064 nm configuration for example) is equal to the ratio of the absorption functions divided by the ratio of the wavelengths. Results obtained with such an energetic approach are consistent with those derived from spectral and temporal LII detection. Furthermore, these results show that the $E(m)$ ratio is constant over a wide range of fluences provided that soot sublimation is not significant. We can thus estimate that this ratio is insensitive to the temperature reached by the particles during and after the laser excitation. This observation is consistent with a recent work from Michelsen et al. [32] indicating that the relative absorption cross section at 532 and 1064 nm is constant from flame temperature up to around 3500 K. Above the sublimation

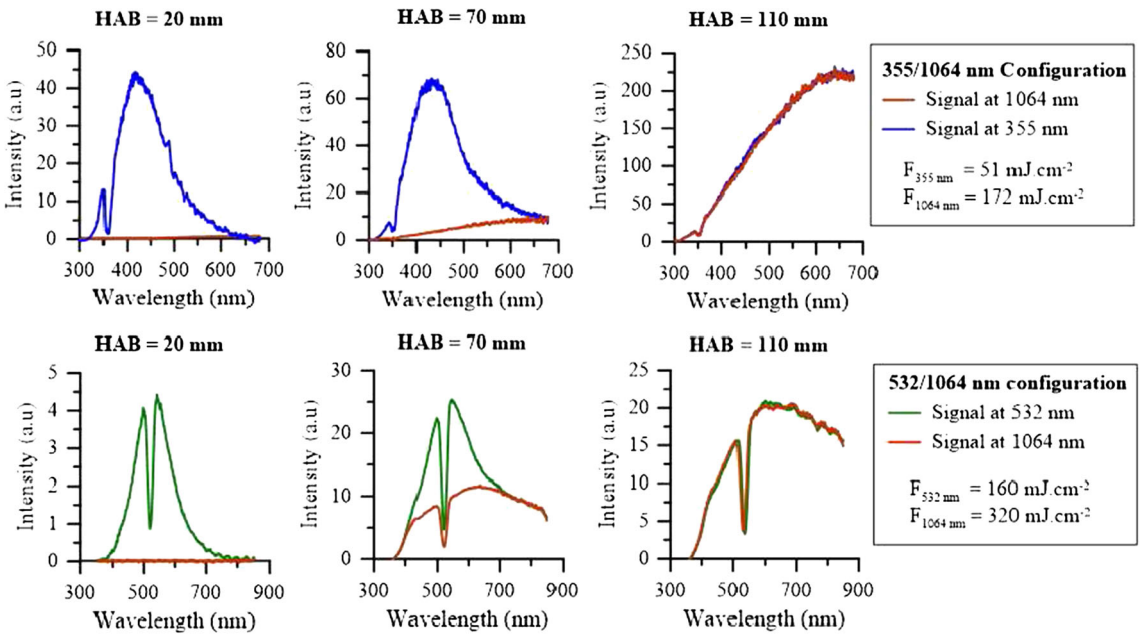

Fig. 6 LII spectra obtained with a prompt detection in a turbulent diesel spray flame at three different heights above the burner using 355/1064 nm and 532/1064 nm configurations

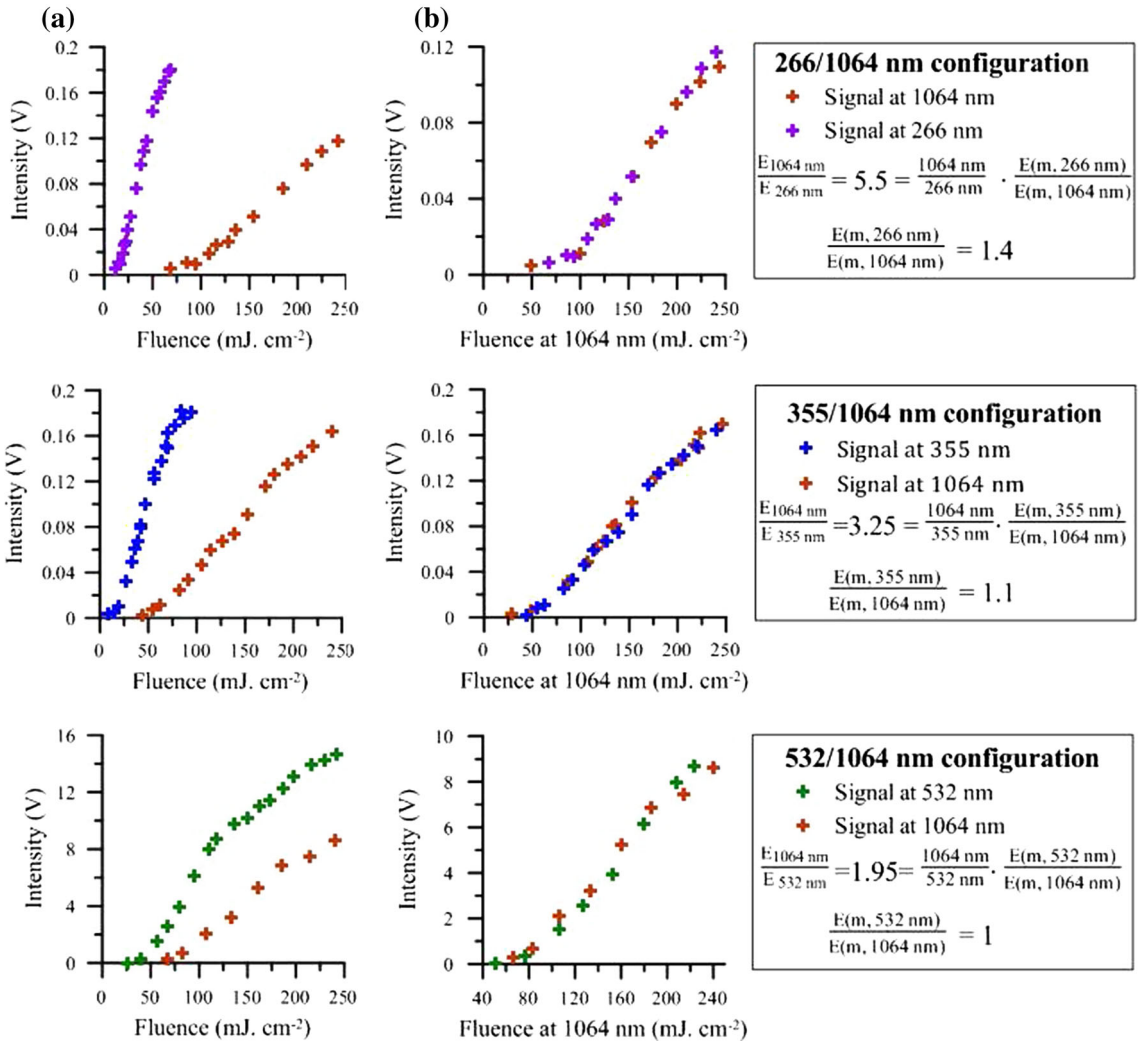

Fig. 7 Fluence curves obtained in the methane premixed flame at 15 mm HAB for the 266/1064 nm, 355/1064 nm and 532/1064 nm configurations (**a**). **b** depicts the same fluence curves when the abscissa values for the 266, 355 and 532 nm signals are multiplied by a correction factor (5.5 for the 266/1064 nm configuration, 3.25 for the 355/1064 nm configuration and 1.95 for the 532/1064 nm configuration) as done in [8, 24]

threshold, these authors observed a significant decrease of the $E(m)$ ratio with increasing fluences. They attributed this trend to molecular interferences that would be expected to interfere differently at 532 and 1064 nm.

5 Conclusions

In this work, we determined the ratios of the soot absorption function using the two-excitation wavelength laser-induced incandescence technique. Measurements have been applied in two types of flames: an atmospheric premixed methane/oxygen/nitrogen flame and a turbulent spray flame of diesel.

- Four pairs of wavelengths have been used to evaluate the relative spectral dependence of the $E(m)$ function. Results show a significant decrease of the $E(m)$ ratio from UV to around 500 nm while it becomes relatively constant for longer wavelengths. This finding is of interest for pyrometric temperature measurements as it validates the use of such a technique when spectral detection bands are chosen beyond 500 nm.
- $E(m)$ ratios have been estimated for different HAB in both flames. The ratio of the soot absorption function seems to be insensitive to HAB in the atmospheric flames studied here. One should note, however, that such a conclusion is limited to the relative evolution of the $E(m)$ function since the two-excitation laser

wavelength technique does not provide information about the absolute value of the soot absorption function.

- $E(m)$ ratios determined in the two investigated flames have been found to be identical suggesting that the ratio of the soot absorption function is insensitive to the fuel type.
- The use of fluence curves to derive the $E(m)$ ratios showed that it can be considered as constant below the sublimation threshold for a wide range of laser fluences. One can thus conclude then that $E(m)$ ratio is also constant from flame temperature up to sublimation temperature which is in agreement with the conclusions drawn by Michelsen et al. [32].

Acknowledgements This work was supported by the Air Quality Program of IRENI (Institut de Recherche en ENvironnement Industriel). The authors thank the Nord-Pas de Calais Region, the Centre Region, the European Funds for Regional Economic Development and the Centre d'Études et de Recherches Lasers et Applications (CERLA) for their financial support.

References

1. H. Horvath, Atmos. Environ. **27**, 293–317 (1993)
2. T.T. Charalampopoulos, J.D. Felske, Combust. Flame **68**(3), 283–294 (1987)
3. T.T. Charalampopoulos, H. Chang, B. Stagg, Fuel **68**(9), 1173–1179 (1989)
4. S.S. Krishnan, K.-C. Lin, G.M. Faeth, ASME J. Heat Transf. **122**(3), 517–524 (2000)
5. S.S. Krishnan, K.-C. Lin, G.M. Faeth, ASME J. Heat Transf. **123**(2), 331–339 (2001)
6. W.H. Dalzell, A.P. Sarofim, ASME J. Heat Transf. **91**(1), 100–104 (1969)
7. T.L. Henriksen, T.A. Ring, D. Call, E.G. Eddings, A.F. Sarofim, 5th U.S. Combustion Meeting, March 25–28th (2007)
8. J. Yon, R. Lemaire, E. Therssen, P. Desgroux, A. Coppalle, K.F. Ren, Appl. Phys. B **104**(2), 253–271 (2010)
9. C.M. Sorensen, Aerosol Sci. Technol. **35**, 648–687 (2001)
10. T.C. Bond, R.W. Bergstrom, Aerosol Sci. Technol. **40**(1), 27–67 (2006)
11. D.R. Snelling, G.J. Smallwood, O.L. Glder, AIAA J. **40**, 1789–1795 (2002)
12. D.R. Snelling, K.A. Thomson, G.J. Smallwood, Appl. Phys. B **96**, 657–669 (2009)
13. B.F. Kock, B. Tribalet, C. Schulz, P. Roth, Combust. Flame **147**, 79–92 (2006)
14. J. Reimann, S.A. Kuhlmann, S. Will, Appl. Phys. B **96**, 583–592 (2009)
15. F. Liu, D.R. Snelling, K.A. Thomson, G.J. Smallwood, Appl. Phys. B **96**, 623–636 (2009)
16. H. Chang, T.T. Charalampopoulos, Proc. R. Soc. Lond. Ser. A **430**, 577–591 (1990)
17. S. Lee, C. Tien, Int. Symp. Combust. **18**(1), 1159–1166 (1981)
18. Z.G. Habib, P. Vervisch, Combust. Sci. Technol. **59**, 261–274 (1988)
19. T.H. Fletch, J. Ma, J.R. Rigby, A.L. Brown, B.W. Webb, Prog. Energy Combust. Sci. **23**, 283–301 (1997)
20. H. Bladh, J. Johnsson, N.-E. Olofsson, A. Bohlin, P.E. Bengtsson, Proc. Combust. Inst. **33**(1), 641–648 (2011)
21. T.L. Farias, M.G. Carvalho, Ü.Ö. Köylü, G.M. Faeth, J. Heat Transf. **117**, 152–159 (1995)
22. CM. Sorensen, J. Cai, N. Lu, Langmuir **8**, 2064–2069 (1992)
23. S. Manickavasagam, M.P. Meng, Appl. Opt. **36**, 1337–1351 (1997)
24. E. Therssen, Y. Bouvier, C. S-Moreau, X. Mercier, P. Desgroux, M. Ziskind, C. Focsa, Appl. Phys. B **89**, 417–427 (2007)
25. R. Lemaire, A. Faccinetto, E. Therssen, M. Ziskind, C. Focsa, P. Desgroux, Proc. Combust. Inst. **32**, 737–744 (2009)
26. R. Lemaire, E. Therssen, P. Desgroux, Fuel **89**, 3952–3959 (2010)
27. G. Cléon, T. Amodeo, A. Faccinnetto, P. Desgroux, Appl. Phys. B **104**, 297–305 (2011)
28. R. Lemaire, S. Bejaoui, E. Therssen, Fuel **107**, 147–161 (2013)
29. H.A. Michelsen, J. Chem. Phys. **118**, 7012–7045 (2003)
30. R. Lemaire, M. Maugendre, T. Schuller, E. Therssen, J. Yon, Rev. Sci. Inst. **80**, 105105–105113 (2009)
31. U. Koylu, G. Faeth, J.Heat Transf. **118**(2), 415–421 (1996)
32. H.A. Michelsen, P.E. Schrader, F. Goulay, Carbon **48**(8), 2175–2191 (2010)
33. H.A. Michelsen, P.E. Schrader, F. Goulay, Carbon **50**(2), 740 (2012)
34. A. D'Anna, Proc. Combust. Inst. **32**, 593–613 (2009)
35. S.De. Iuliis, S. Maffi, F. Cignoli, G. Zizak, Appl. Phys. B **102**(4), 891–903 (2010)
36. F. Migliorini, S.De. Iuliis, S. Maffi, F. Cignoli, G. Zizak, Appl. Phys. B **96**, 637–643 (2009)